Research on Dynamic Modeling and Parameter Influence of Adaptive Gun Head Jet System of Fire-Fighting Monitor

XIAOMING YUAN[ID]1,2,3, **XUAN ZHU**[ID]1,3, **CHU WANG**[ID]1,3, **AND LIJIE ZHANG**[ID]1,3

[1]Hebei Key Laboratory of Heavy Machinery Fluid Power Transmission and Control, Yanshan University, Qinhuangdao 066004, China
[2]State Key Laboratory of Fluid Power and Mechatronic Systems, Zhejiang University, Hangzhou 310027, China
[3]Key Laboratory of Advanced Forging and Stamping Technology and Science, Ministry of Education of China, Yanshan University, Qinhuangdao 066004, China

Corresponding authors: Chu Wang (wangchu@stumail.ysu.edu.cn) and Lijie Zhang (zhangljys@126.com)

ABSTRACT The jet medium of the adaptive gun head jet system of the fire-fighting monitor is generally a mixture of air and water. During the operation, the equivalent stiffness of the jet fluid fluctuates periodically or randomly due to the pressure pulsation of the jet system and the external excitation such as wind, thus the dynamic behavior of the adaptive gun head jet system of the fire-fighting monitor has typical nonlinear characteristics. In this paper, based on the assumption that the equivalent stiffness of the fluid fluctuates in type of simple harmonic motion, a nonlinear dynamic model of the jet system is established, and the model is solved by the multi-scale method. The influence of design parameters such as fluid pulsation frequency, air inlet rate and fluid pressure on the amplitude of the main resonance and combined resonance of the jet system is analyzed. Results show that the existence of the fluid pulsation frequency increases the resonance frequency range of the jet system. As to the influence of design parameters on the dynamic characteristics of the jet system, from the point of view of amplitude change, the air inlet rate has the greatest impact on the main resonance, and the fluid pulsation frequency has the dominant influence on the combined resonance. This research can provide theoretical support for the dynamic optimization of the adaptive gun head jet system of the fire-fighting monitor.

INDEX TERMS Fire-fighting monitor, adaptive gun head, jet system, parameter vibration, parameter influence.

I. INTRODUCTION

Compared with the fixed nozzle opening gun head, the nozzle opening of the adaptive gun head can be adjusted by an adaptive mechanism to match the parameters of the jet system such as the pressure and the flow. Therefore, the fire-fighting monitor with adaptive gun head has the advantages of wide flow range, long range and high stability, which can meet more fire needs [1]. In addition, early warning fire detection and fire video image detection are also used to reduce personal damage and property loss [2], [3]. The working medium of the adaptive gun head jet system of the

fire-fighting monitor is generally water containing a certain amount of air, i.e., the gas-liquid mixed fluid. The fire pump is the power source of the jet system, and he flow and pressure pulsation may occur under its start, stop and normal working conditions. Therefore, the air mixed in the fluid will inevitably dissolve or release, resulting in the constant change of the compressibility and the equivalent stiffness of the fluid, which affects the modal characteristics of the jet system and finally influences the steady-state and dynamic performance of the jet system [4]. Similarly, when the fire-fighting monitor operates outdoors, there may be random excitation such as wind, which makes dynamic behavior of the jet system more complicated [5]. Since the fluid state parameters vary periodically or randomly affected by the fluid compressibility and

The associate editor coordinating the review of this manuscript and approving it for publication was Lei Wang.

pressure pulsation, the adaptive gun head jet system of fire-fighting monitor is a non-autonomous system [6]–[8].

There are three kinds of pressure pulsation components in the fire pump: random pulsation, blade-passing frequent pulsation and rotation frequent pulsation [9]. The pressure pulsation of the fire pump is closely related to the relative movement of the impeller and guide vane of the pump, and is affected by the secondary flow and cavitation in the pump. The pressure pulsation can be applied in mensuration at best efficiency point, monitoring outlet pressure, and fault diagnosis and prevention [10], [11]. Some scholars have also researched on the pressure pulsation mechanism of hydrodynamic components. Li *et al.* calculated the unsteady flow and pressure fluctuation characteristics of the mixed flow pump based on the shear stress transport (SST) turbulence model [12]. Li *et al.* simulated the closing process of the guide vanes in a pump-turbine by the dynamic mesh method, and analyzed the flow characteristics and pressure fluctuations [13].

Pulsation and resonance are ubiquitous [14], and in the research of nonlinear vibration, research objects often have uncertainty and interference [15]. Scholars usually utilize nonlinear dynamic theory and methods to carry out relevant research, such as Poincare map, time history [16], power spectral density and multi-scale method etc. [17], [18]. There are also literatures on improving the stability, accuracy, and rapidity of the fluid transmission and control system. Zhu *et al.* established a closed-loop control system and introduced the Popov frequency criterion method for system stability judgment [19]. Lyu *et al.* proposed a novel pump-valve system and applied robust control approach [20], [21]. Some scholars constructed state observers [22], or developed an advanced nonlinear controller for hydraulic system [23] to improve the efficiency of fluid systems.

In the dynamic analysis, the design and state parameters of the system have a non-negligible effect on the dynamic characteristics of the system. For the analysis of the dynamic parameters and the optimization design, scholars have many research achievements. Methods like sensitivity analysis [24], numerical simulation [25], and feedback linearization etc. [26] have been applied by scholars in studying the influence analysis of dynamic system parameters. In terms of parameter optimization, multi-factor design optimization has become the major research direction. Pei *et al.* utilized a multi-objective genetic algorithm to obtain the best optimized objectives as well as the best combination of design parameters [27]. This method of establishing a model between design variables and performance functions and using genetic optimization algorithms to solve the problem is widely used in actual engineering [28], [29]. In addition, the response surface method, as an optimization method combining experimental design and mathematical modeling, has also been used in optimization problems. Rafiee and Faiz proposed a surrogate model using the response surface method integrated with the particle swarm optimization, which improved the effectiveness of the robust optimization of the outer rotor permanent magnet motor [30]. Hazir *et al.* integrated

response surface method, desirability function and genetic algorithm techniques for optimization of computer numerical control (CNC) machining parameters, and experimental results showed that the approach could minimize the surface roughness value of beech species efficiently [31].Effective parameter estimation models also play an important role in optimal design. The Kriging model is an unbiased estimation model with the smallest estimated variance, which can well approximate complex problems with nonlinear characteristics [32]. Ni *et al.* applied Kriging method on reliability analysis of RC structures and steel frame structures and demonstrated the efficiency of the method for complex engineering problems [33]. In the adaptive gun head jet system of the fire-fighting monitor, the design parameters will have impacts on the dynamic characteristics of the jet system, but the corresponding influencing laws still need to be revealed.

In summary, the pressure pulsation inevitably occurs during the operation of the adaptive gun head jet system of the fire-fighting monitor, which makes the system have obvious nonlinear characteristics and affect the jet performance. At present, there are few literatures on the dynamics of the adaptive gun head jet system of the fire-fighting monitor and the research on the nonlinear dynamic characteristics of the jet system has not been carried out. Therefore, based on the multi-scale method, the nonlinear dynamics of the adaptive gun head jet system of the fire-fighting monitor is planned to be analyzed; By substituting the known parameters of the jet system into the derived parametric vibration equation, the numerical simulation is carried out using the Runge-Kutta method, then and the influence law of the design parameters such as the fluid pulsation frequency, air inlet rate, and fluid pressure on the response amplitude of the main resonance and combined resonance of the jet system is to be revealed, which can provide a reference for the design optimization of the adaptive gun head jet system of the fire-fighting monitor.

This paper is organized as follows. In Section II, the dynamic model of the adaptive gun head jet system of the fire-fighting monitor is established. In Section III, the parametric vibration equation of the jet system is derived by the multi-scale method. Section IV analyzes the influence of different parameters on the response of jet system parametric vibration. Section V draws the conclusions. The flow chart is shown in Fig. 1.

II. DYNAMIC MODEL OF JET SYSTEM

The structure of the adaptive gun head of fire-fighting monitor is shown in Fig. 2. The inlet of the gun head is on the left side and the outlet is on the right. The adaptive mechanism consisting of the spray core, the end cap, the core rod, and the spring is the core component of the adaptive gun head. The end cap and the core rod are fixedly connected to the enclosure through the regulator. The spray core can slide in the axial direction. The left side of the spring acts on the spray core and the right side acts on the end cap. At the initial moment, the spring is in a pre-compressed state. Meanwhile, the spray core is closely attached to the inner nozzle and
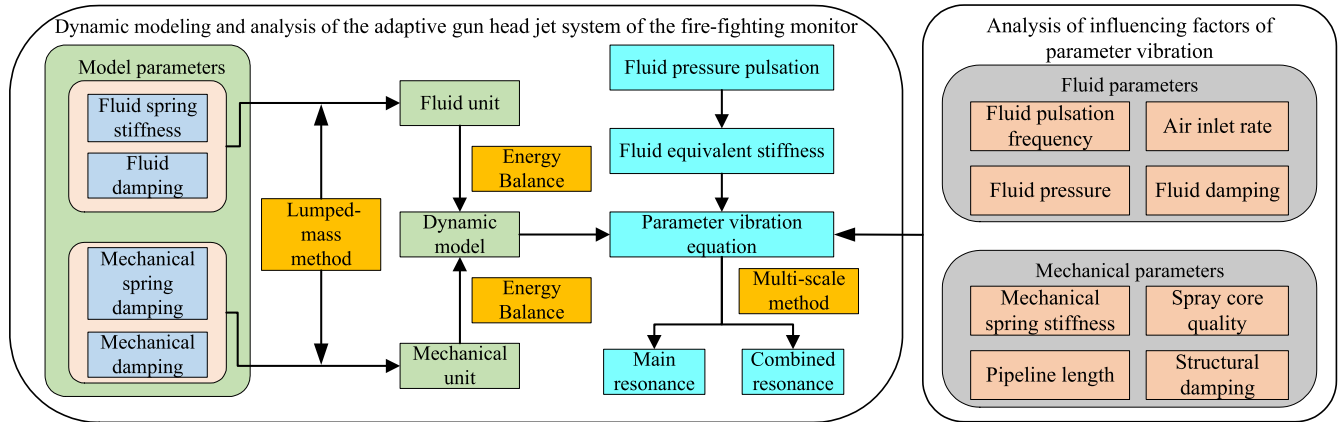
FIGURE 1. The flow chart.

Notations			
F	:External excitation amplitude	m_1	:Mass of fluid unit 1
m_2	:Mass of spray core	m_3	:Mass of fluid unit 2
k_{f1}	:Stiffness of fluid unit 1	k_{f21}	:Part of stiffness of fluid unit 2
k_{f22}	: Part of stiffness of fluid unit 2	k_1	:Stiffness of mechanical spring
c_1	: Fluid damping	c_2	:Structural damping
c_{21}	: Part of structural damping	c_{22}	:Part of structural damping
p	:Time-varying pressure pulsation	$\bar{p}$	:Steady pressure
Δp	:Pressure pulsation amplitude	ω_o	:Pressure pulsation angular frequency
S_a	:Flow section of the fluid element	l	:Axial length of the fluid domain
p_0	:Initial pressure	ΔF	:$S_a(p_0-p)$
k_{fi}	:Fluctuation of equivalent fluid stiffness	$\bar{k}_{fi}$	:Steady equivalent stiffness of the fluid unit
Δk_{fi}	:Fluctuation of equivalent fluid unit stiffness	ε	:$\Delta k_{fi} / 2\bar{k}_{fi}$
ω_f	:Equivalent stiffness fluctuating frequency of fluid units	ψ	:Regular mode
Λ	:Spectral matrix	η	:Regular displacement vector
C_N	:Regular damping matrix	ΔQ	:Regular external excitation vector
ΔK_N	:Regular equivalent stiffness fluctuation matrix of the fluid unit	C'_N	:C_N/ε
F'	:F/ε	σ	:Tuning parameter
θ	:$\arctan(c'_{N11}/2\sigma)$	A_1	:Calculation coefficient
B_1	:Calculation coefficient	D_1	:Calculation coefficient
B_f	:Steady value of dynamic bulk modulus of gas-liquid mixed fluid	ΔB_f	:Fluctuating value of dynamic bulk modulus of gas-liquid mixed fluid

the nozzle opening is zero. When the inlet flow increases, the pressure on the left side of the spray core increases. If the pressure is greater than the spring preload, the spray core will move to the right and the nozzle opening increases. Otherwise it will move to the left and the nozzle opening will decrease. The adaptive gun head can automatically adjust the nozzle opening according to the changes of the inlet flow and pressure, so that it can achieve the best or near-optimal performance under various flows, and extinguish large fires quickly and efficiently.

The internal structure of the adaptive gun head of the fire-fighting monitor is shown in Fig. 3, and the pipe sections and their cross-sectional dimensions are shown in Table 1.

In Fig. 3, the red line with arrows is the fluid flow line. According to the direction of the flow line, the fluid flows through the n-n section where the nozzle opening is located,
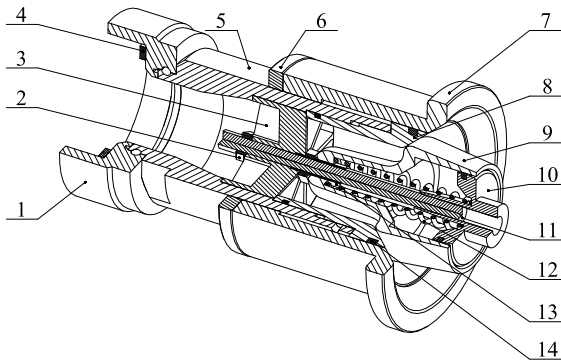
FIGURE 2. Structure of adaptive gun head. 1. Joint, 2. Nut, 3. Regulator, 4. Gasket, 5. Enclosure, 6. Ring, 7. Outer nozzle, 8. Inner nozzle, 9. Spray core, 10. End cap, 11. Core rod, 12. Spring, 13. Core sleeve, 14. Seal ring.
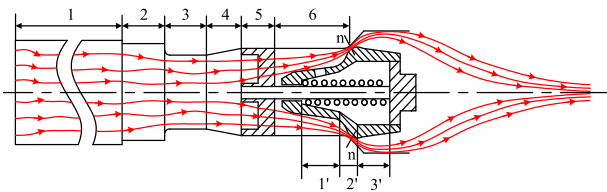

FIGURE 3. Internal profile and streamline of the adaptive gun head of the fire-fighting monitor.

TABLE 1. Internal structure size of the adaptive gun head of the fire-fighting monitor.

Fluid unit	Segmentation	Average area of flow cross section S_a/(mm^2)	Axial length of the fluid domain l/mm
	1	6221	1534.6
	2	6200	38
Fluid unit 1	3	3200	39
	4	3800	35.5
	5	4400	38
	6	3700	64
	1'	300	46.1
Fluid unit 2	2'	800	11
	3'	2800	40.5

and then is reflected by the inner surface of the outer nozzle to converge at the front end of the fire-fighting monitor and form a jet. The regulator is installed at the fifth section of gun head as show in Fig. 3, which can reduce the jet vortex and convert the radial velocity of the fluid to the axial velocity, so that the jet tends to be laminar flow and the range of the fire-fighting monitor is improved. At the center of the spray core guidance surface, there are circular holes distributed evenly along the circle. During the operation of the fire-fighting monitor, the fluid enters the interior of the spray core through circular holes and forms a certain hydrostatic pressure.

In order to facilitate theoretical modeling and analysis, the dynamic model of the adaptive gun head jet system of fire-fighting monitor makes the following assumptions:

1. Except the fluid unit and the spring, the spray core, the enclosure, and the pipes are considered to be rigid bodies and their deformation under pressure pulsation is not considered.

2. The spray core and the fluid are only subjected to the axial force, and the force of the fluid on the spray core is simplified to the spring force along the axial direction.

3. The damping between the fluid unit and the solid unit is equivalent to the axial linear damping, and the damping formed by the uniformly distributed small hole on the nozzle is equivalent to the axial linear damping.

4. Processing and installation errors of the jet system are ignored.

The dynamic model of the adaptive gun head jet system of the fire-fighting monitor is shown in Fig. 4.
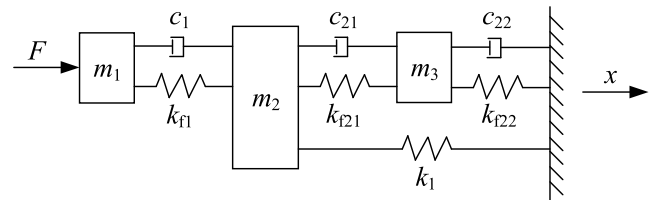

FIGURE 4. Dynamic model of the adaptive gun head jet system of the fire-fighting monitor.

In Fig. 4, F is the pulsating excitation force caused by the pressure fluctuation of the fire pump. m_1, m_2, and m_3 are the masses of the fluid unit 1, the spray core and the fluid unit 2 in the jet system, respectively. The fluid unit 1 is the fluid contained by the inlet flow cross section, the outer surface of the spray core, and the flow cross section n-n of the jet system, along with the internal surface of the fire-fighting monitor parts. The fluid unit 2 is the fluid contained by the inner surface of the spray core and the left end surface of the end cap. k_{f1} is the stiffness of fluid unit 1. k_{f21} is equal to k_{f22}, the total stiffness obtained by paralleling the two is the stiffness of fluid unit 2. k_1 is the stiffness of the mechanical spring inside the spray core. c_1 is the equivalent linear damping between the pipe wall and the outer wall of the monitor and the fluid unit 1 in the jet system. c_{21} is equal to c_{22}, and the total damping obtained by paralleling the two is equivalent to the structural damping of the orifice of the spray core.

III. DERIVATION AND SOLUTION OF VIBRATION EQUATION OF JET SYSTEM
A. PARAMETRIC VIBRATION EQUATION OF JET SYSTEM
Under actual conditions, the pulsation of the flow and pressure of the fire pump is inevitable, so the fluid density and equivalent stiffness constantly change. The fluid pressure consists of two parts during the operation: steady-state pressure and dynamic pressure. Assuming that the pulsating pressure varies by cosine, according to Euler's theorem, the time-varying pressure pulsation can be expressed as:

$$p = \bar{p} + \Delta p \left(e^{j\omega_o t} + e^{-j\omega_o t} \right) \tag{1}$$

where $\bar{p}$ is steady pressure, Δp is the pressure pulsation amplitude (Pa), and ω_o is the pressure pulsation angular frequency (rad/s).

Assuming that the average area of the flow section of the fluid element is S_a and the axial length of the fluid domain is

l, then the definition of stiffness can be expressed as:

$$k_f = -\frac{\Delta F}{\Delta l} \quad (2)$$

where $\Delta F = S_a(p_0 - p)$, and p_0 is the initial pressure.

Therefore, the stiffness of fluid is the function of the fluid pressure. Similar to the fluid pressure, the fluctuation of the equivalent fluid stiffness can be expressed as:

$$k_{fi} = \bar{k}_{fi} + \Delta k_{fi} \cos \omega_f t = \bar{k}_{fi} \left(1 + \varepsilon e^{j\omega_f t} + \varepsilon e^{-j\omega_f t}\right) \quad (3)$$

where $i = 1, 2$, $\bar{k}_{fi}$ is the steady equivalent stiffness of the fluid unit (N/m), Δk_{fi} is the equivalent stiffness fluctuation of the fluid unit (N/m), ε is a small parameter and $\varepsilon = \Delta k_{fi}/2\bar{k}_{fi}$, and ω_f is the time-varying equivalent stiffness angular frequency of the fluid unit (rad/s).

The regular mode ψ and the spectral matrix Λ of the system are known, after regularizing the dynamic equation of parametric vibration of the jet system by referring [9], we can get:

$$\ddot{\eta} + C_N \dot{\eta} + \Lambda \eta = \Delta Q - \Delta K_N \eta \quad (4)$$

where η is the regular displacement vector, C_N is the regular damping matrix, ΔQ is the regular external excitation vector and ΔK_N is the regular equivalent stiffness fluctuation matrix of the fluid unit.

Among them, C_N is:

$$C_N = \begin{bmatrix} c_{N11} & c_{N12} & c_{N13} \\ c_{N21} & c_{N22} & c_{N23} \\ c_{N31} & c_{N32} & c_{N33} \end{bmatrix} \quad (5)$$

ΔQ can be expressed as:

$$\Delta Q = F \frac{\left(e^{j\omega_f t} + e^{-j\omega_f t}\right)}{2} \begin{bmatrix} \psi_{1,1} & \psi_{1,2} & \psi_{1,3} \end{bmatrix}^T \quad (6)$$

And ΔK_N is:

$$\Delta K_N = \varepsilon \left(e^{j\omega_f t} + e^{-j\omega_f t}\right) \begin{bmatrix} \Delta k_{N11} & \Delta k_{N12} & \Delta k_{N13} \\ \Delta k_{N21} & \Delta k_{N22} & \Delta k_{N23} \\ \Delta k_{N31} & \Delta k_{N32} & \Delta k_{N33} \end{bmatrix} \quad (7)$$

B. APPROXIMATE ANALYTICAL SOLUTION OF THE MAIN RESONANCE OF JET SYSTEM

The quadratic approximate solution and small parameter are introduced based on the multi-scale method:

$$\begin{cases} \eta_i = \eta_{i0}(T_0, T_1) + \varepsilon \eta_{i1}(T_0, T_1) + \cdots \\ c_{Nij} = \varepsilon c'_{Nij} \\ F = \varepsilon F' \end{cases} \quad (8)$$

where $T_0 = t$, $T_1 = \varepsilon t$, and values of i and j are 1, 2, and 3, respectively.

Substituting the above equations into (4), we obtain the steady-state response of the main resonance of the jet system:

$$x = \psi (\eta_0 + \varepsilon \eta_1) \quad (9)$$

where, the steady zero-order approximate analytical solution of the jet system is:

$$\begin{cases} \eta_{10} = -\dfrac{F'\psi_{1,1}}{\omega_{n1}\sqrt{(c'_{N11})^2 + 4\sigma^2}} \cos\left(\theta + (\omega_{n1} + \varepsilon\sigma)t\right) \\ \eta_{20} = 0 \\ \eta_{30} = 0 \end{cases} \quad (10)$$

where, σ is the tuning parameter and $\theta = \arctan\left(c'_{N11}/2\sigma\right)$.

The steady first-order approximate analytical solution of the jet system is:

$$\begin{cases} \eta_{11} = -2\Delta k_{N11}A_1 \begin{bmatrix} \dfrac{\cos(\omega_{n1} - \omega_f)t}{\omega_f(2\omega_{n1} - \omega_f)} \\ -\dfrac{\cos(\omega_{n1} + \omega_f)t}{\omega_f(2\omega_{n1} + \omega_f)} \end{bmatrix} \\ \eta_{21} = \dfrac{F'\psi_{1,2}\cos(\omega_o t)}{\omega_{n2}^2 - \omega_o^2} \\ \qquad -2 \begin{bmatrix} \Delta k_{N21}A_1 \left(\dfrac{\cos(\omega_{n1} + \omega_f)t}{\omega_{n2}^2 - (\omega_{n1} + \omega_f)^2} \\ +\dfrac{\cos(\omega_{n1} - \omega_f)t}{\omega_{n2}^2 - (\omega_{n1} - \omega_f)^2}\right) \\ -\dfrac{c'_{N21}\omega_{n1}A_1 \sin\omega_{n1}t}{\omega_{n2}^2 - \omega_{n1}^2} \end{bmatrix} \\ \eta_{31} = \dfrac{F'\psi_{1,3}\cos(\omega_o t)}{\omega_{n3}^2 - \omega_o^2} \\ \qquad -2 \begin{bmatrix} \Delta k_{N31}A_1 \left(\dfrac{\cos(\omega_{n1} + \omega_f)t}{\omega_{n3}^2 - (\omega_{n1} + \omega_f)^2} \\ +\dfrac{\cos(\omega_{n1} - \omega_f)t}{\omega_{n3}^2 - (\omega_{n1} - \omega_f)^2}\right) \\ -\dfrac{c'_{N31}\omega_{n1}A_1 \sin\omega_{n1}t}{\omega_{n3}^2 - \omega_{n1}^2} \end{bmatrix} \end{cases} \quad (11)$$

where, A_1 is a coefficient in calculating the steady zero-order approximate analytical solution of the jet system.

Similarly, the main resonance response of the jet system can also be solved when the external excitation frequency is close to the second and third natural frequencies respectively.

C. APPROXIMATE ANALYTICAL SOLUTION OF THE COMBINED RESONANCE OF JET SYSTEM

The multi-scale method can also be used to derive the combined resonance response of the jet system. The small parameter is introduced and the quadratic approximate solution is assumed as follows:

$$\begin{cases} \eta_i = \eta_{i0}(T_0, T_1) + \varepsilon \eta_{i1}(T_0, T_1) + \cdots \\ c_{Nij} = \varepsilon c'_{Nij} \end{cases} \quad (12)$$

where, $T_n = \varepsilon^n t$ and values of i and j are 1, 2, and 3, respectively.

Substituting the above equations into (4), we obtain the steady-state response of the combined resonance of the jet system:

$$x = \psi (\eta_0 + \varepsilon \eta_1) \quad (13)$$

where the steady zero-order approximate analytical solution of the combined resonance is:

$$
\begin{cases}
\begin{aligned}
\eta_{10} = {} & 2\frac{(\Delta k_{N11}D_1 + \Delta k_{N12}D_2 + \Delta k_{N13}D_3)}{\omega_{n1}\sqrt{4\sigma^2 + (c'_{N11})^2}} \\
& \times \cos\left(\theta + (\omega_{n1} + \varepsilon\sigma)\,t\right) \\
& + 2D_1\cos\omega_o t
\end{aligned} \\
\eta_{20} = 2D_2\cos\omega_o t \\
\eta_{30} = 2D_3\cos\omega_o t
\end{cases}
\tag{14}
$$

The steady first-order approximate analytical solution of the jet system is (15), as shown at the bottom of the page, where, B_1 and D_1 are coefficients in calculating the steady zero-order approximate analytical solution of the jet system.

Similarly, the combined resonance response of the jet system can also be solved when the external excitation frequency is close to the combined frequency between the natural frequencies of the second and third order and the equivalent stiffness fluctuation frequency of the fluid unit respectively.

IV. ANALYSIS OF INFLUENCING FACTORS OF PARAMETER VIBRATION OF JET SYSTEM

The parameter vibration response of the jet system is mainly affected by parameters such as the fluid pulsation frequency, the air inlet rate, the fluid pressure, the spray core quality, the mechanical spring stiffness, the fluid damping, the structural damping, and the pipeline length. By changing the value of each parameter, the influence law of different design parameters on the vibration response of the jet system can be determined. The parameters required for the parameter vibration calculation of the jet system are shown in Table 2.

A. INFLUENCE OF FLUID PULSATION FREQUENCY ON PARAMETER VIBRATION RESPONSE OF JET SYSTEM

By taking the parameters shown in Table 2 into the steady-state response equation of the combined resonance of the jet system, when the external excitation frequency is close to the combined frequency between the first natural frequency

$$
\begin{cases}
\eta_{11} = -2\left[\Delta k_{N11}B_1\left(\dfrac{\cos(\omega_{n1}-\omega_f)t}{\omega_f(2\omega_{n1}-\omega_f)} - \dfrac{\cos(\omega_{n1}+\omega_f)t}{\omega_f(2\omega_{n1}+\omega_f)}\right) + \dfrac{(\Delta k_{N11}D_1 + \Delta k_{N12}D_2 + \Delta k_{N13}D_3)\cos(\omega_o+\omega_f)t}{(\omega_{n1}^2 - (\omega_o+\omega_f)^2)} - \dfrac{\omega_o(c'_{N11}D_1 + c'_{N12}D_2 + c'_{N13}D_3)\sin\omega_o t}{(\omega_{n1}^2 - \omega_o^2)}\right] \\[4em]
\eta_{21} = -2\left[\Delta k_{N21}B_1\left(\dfrac{\cos(\omega_{n1}+\omega_f)t}{\omega_{n2}^2 - (\omega_{n1}+\omega_f)^2} + \dfrac{\cos(\omega_{n1}-\omega_f)t}{\omega_{n2}^2 - (\omega_{n1}-\omega_f)^2}\right) + (\Delta k_{N21}D_1 + \Delta k_{N22}D_2 + \Delta k_{N23}D_3)\left(\dfrac{\cos(\omega_o+\omega_f)t}{\omega_{n2}^2 - (\omega_o+\omega_f)^2} + \dfrac{\cos(\omega_o-\omega_f)t}{\omega_{n2}^2 - (\omega_o-\omega_f)^2}\right) - \dfrac{\omega_o(c'_{N21}D_1 + c'_{N22}D_2 + c'_{N23}D_3)\sin\omega_o t}{\omega_{n2}^2 - \omega_o^2} - \dfrac{\omega_{n1}c'_{N21}B_1\sin\omega_{n1}t}{\omega_{n2}^2 - \omega_{n1}^2}\right] \\[4em]
\eta_{31} = -2\left[\Delta k_{N31}B_1\left(\dfrac{\cos(\omega_{n1}+\omega_f)t}{\omega_{n3}^2 - (\omega_{n1}+\omega_f)^2} + \dfrac{\cos(\omega_{n1}-\omega_f)t}{\omega_{n3}^2 - (\omega_{n1}-\omega_f)^2}\right) + (\Delta k_{N31}D_1 + \Delta k_{N32}D_2 + \Delta k_{N33}D_3)\left(\dfrac{\cos(\omega_o+\omega_f)t}{\omega_{n3}^2 - (\omega_o+\omega_f)^2} + \dfrac{\cos(\omega_o-\omega_f)t}{\omega_{n3}^2 - (\omega_o-\omega_f)^2}\right) - \dfrac{\omega_o(c'_{N31}D_1 + c'_{N32}D_2 + c'_{N33}D_3)\sin\omega_o t}{\omega_{n3}^2 - \omega_o^2} - \dfrac{\omega_{n1}c'_{N31}B_1\sin\omega_{n1}t}{\omega_{n3}^2 - \omega_{n1}^2}\right]
\end{cases}
\tag{15}
$$

TABLE 2. Parameters of adaptive gun head jet system of the fire-fighting monitor.

Parameter	Symbol	Unit	Value
Mass of fluid unit 1	m_1	kg	10.4
Mass of spray core	m_2	kg	0.32
Mass of fluid unit 2	m_3	kg	0.14
Steady value of dynamic bulk modulus of gas-liquid mixed fluid	B_f	Mpa	161.92
Fluctuating value of dynamic bulk modulus of gas-liquid mixed fluid	ΔB_f	Mpa	0.34
Equivalent stiffness steady value of fluid unit 1	$\bar{k}_{f1}$	kN/m	541.15
Equivalent stiffness fluctuating value of fluid unit 1	Δk_{f1}	kN/m	1.14
Equivalent stiffness steady value of fluid unit 2	$\bar{k}_{f2}$	kN/m	852.22
Equivalent stiffness fluctuating value of fluid unit 2	Δk_{f2}	kN/m	1.79
Equivalent stiffness fluctuating frequency of fluid units	ω_f	rad·s^{-1}	294.01
Stiffness of mechanical spring	k_1	kN/m	18
External excitation amplitude	F	N	4.26
Fluid damping	c_1	N·(m/s)$^{-1}$	0.01
Structural damping	c_2	N·(m/s)$^{-1}$	0.05

FIGURE 5. Combined resonance response jet system when ω_f is 10Hz. (a) time domain response. (b) frequency domain response.

and the fluid pulsation frequency, the time domain response and frequency domain response of the combined resonance of the jet system under different fluid pulsation frequencies are shown in Fig. 5, Fig. 6, and Fig. 7, respectively.

It can be seen from the time-domain response graphs in Fig. 5, Fig.6, and Fig. 7 that as the fluid pulsation frequency gradually increases, the steady-state amplitude of each degree of freedom of the jet system gradually decreases under the effect of the combined frequency. The combined frequency includes the first natural frequency, so x_1, i.e., the amplitude of the fluid unit 1 is the largest, the amplitude of the spray core is the second, and the amplitude of the fluid unit 2 is the smallest, which is determined by the mode vector corresponding to the first natural frequency of the jet system. It can be seen from the frequency domain response graphs in Fig. 5, Fig. 6, and Fig. 7 that there are four peaks when the combined resonance of the jet system occurs. The frequency corresponding to each peak is consistent with the approximate analytical formula of the combined resonance of the jet system. The first natural frequency corresponds to the largest peak, indicating that the natural frequency plays a dominant role in the combined resonance, and the remaining frequencies have effects of regulation. It can be seen from Fig. 5 (b) that on the left side of the peak corresponding to the first natural frequency there exists a very low peak, the frequency corresponding to which is $\omega_{n1} - \omega_f$; On the right side of the highest peak there are two peaks, and the frequency corresponding to the left one is ω_o, and the frequency corresponding to the right one is $\omega_o + \omega_f$. It can be known from Fig. 6 (b) and Fig. 7 (b) that on the right side of the peak corresponding to the first natural frequency there are three peaks, of which the frequency corresponding to the left one is $-(\omega_{n1} - \omega_f)$, the frequency corresponding
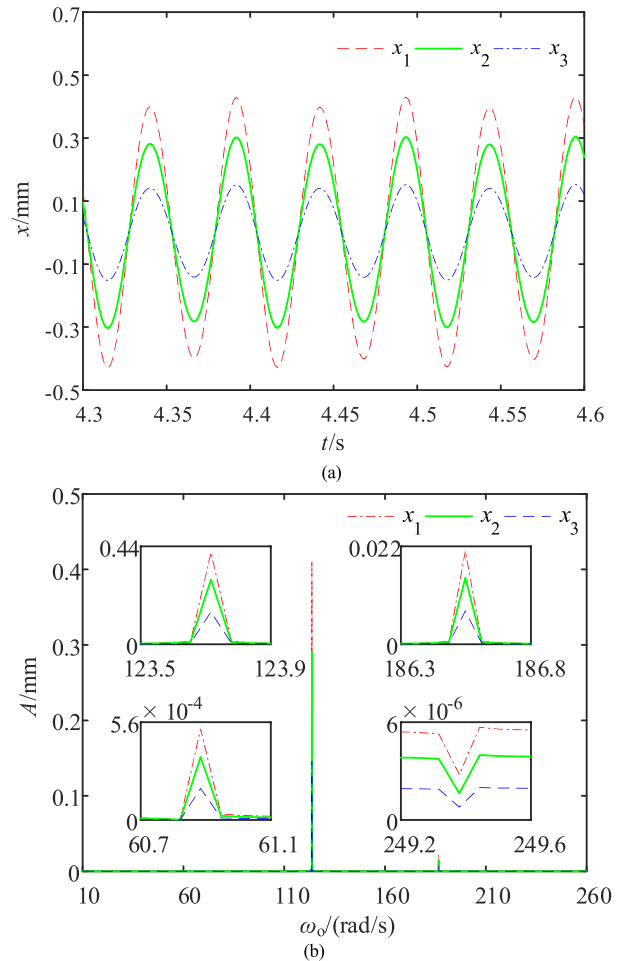
to the central one is ω_o, and the frequency corresponding to the right one is $\omega_o + \omega_f$. From the above analysis, it can be seen that the combined frequency plays a major role among the three frequencies that regulate the combined resonance of the jet system.

When the external excitation frequency is close to the combined frequency between the second natural frequency and the fluid pulsation frequency, the time domain response and frequency domain respo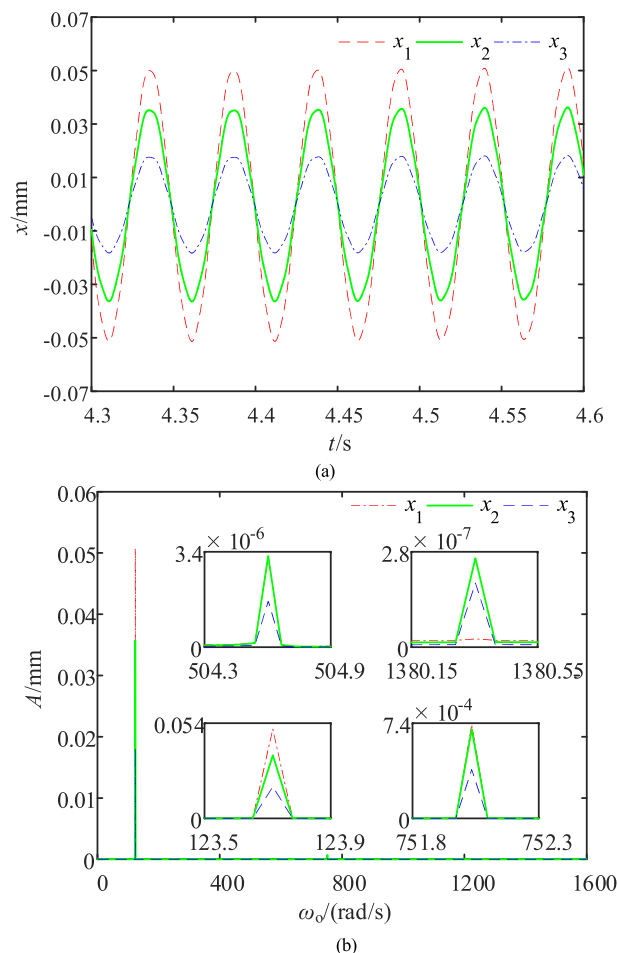nse of the combined resonance of the jet system under different fluid pulsation frequencies are shown in Fig. 8, Fig. 9, and Fig. 10, respectively.

It can be seen from the time-domain response graphs in Fig. 8, Fig. 9, and Fig. 10 that as the fluid pulsation frequency gradually increases, the steady-state amplitude of each degree of freedom of the jet system gradually decreases under the effect of the combined frequency. The combined frequency includes the second natural frequency, so x_2, i.e., the amplitude of the spray core is the largest, the amplitude of the fluid unit 2 is the second, and the amplitude of the fluid unit 1 is the smallest, which is determined by the mode vector corresponding to the second natural frequency of the jet system. It can be seen from the frequency domain response graphs in Fig. 8, Fig. 9, and Fig. 10 that there are four peaks
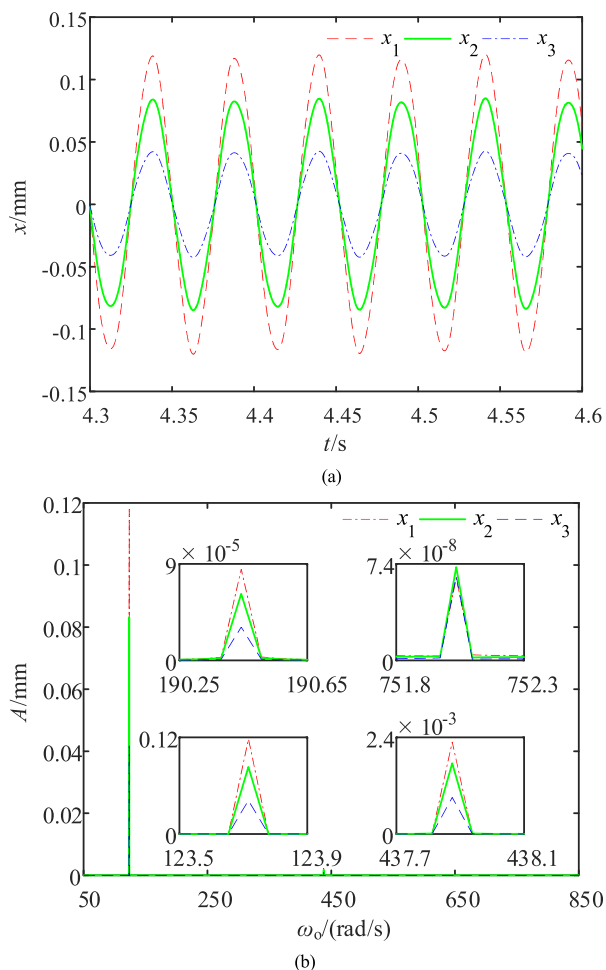
FIGURE 6. Combined resonance response jet system when ω_f is 50Hz. (a) time domain response. (b) frequency domain response.

FIGURE 7. Combined resonance response jet system when ω_f is 100Hz. (a) time domain response. (b) frequency domain response.

when the combined resonance of the jet system occurs. The frequency corresponding to each peak is consistent with the approximate analytical formula of the combined resonance of the jet system. The second natural frequency corresponds to the largest peak, indicating that the natural frequency plays a dominant role in the combined resonance, and the remaining frequencies have effects of regulation. It can be seen from Fig. 8 (b) that there are three lower peaks near the peak corresponding to the natural frequency, one is on the left and the other two are on the right side, and the frequency corresponding to the left one is $\omega_2 - \omega_f$, while the frequencies corresponding to the other two are ω_o and $\omega_o + \omega_f$, respectively. The variation law of the frequency domain response shown in Fig. 9 (b) and Fig. 10 (b) is the same as that in Fig. 8 (b). From the above analysis, it can be seen that the combined frequency plays a major role among the three frequencies that regulate the combined resonance of the jet system.

When the external excitation frequency is close to the combined frequency between the third natural frequency and the fluid pulsation frequency, the time domain response and frequency domain response of the combined resonance of

the jet system under different fluid pulsation frequencies are shown in Fig. 11, Fig. 12, and Fig. 13, respectively.

The variation law of the combined resonance response shown in Fig. 11, Fig. 12, and Fig. 13 is the same as that in Fig. 8, Fig. 9, and Fig. 10. By comparing the above amplitude-frequency characteristic curves, it can be seen that the existence of fluid pulsation frequency increases the resonance frequency range of the jet system.

When the fluid pulsation frequency is changed, the variation law of the main resonance response of the jet system is basically consistent with that of the combined resonance response. When the fluid pulsation frequency continuously changes and the external excitation frequency is close to the first natural frequency and the combined frequency between the first natural frequency and the fluid pulsation frequency respectively, the variation curves of the main resonance and combined resonance amplitude of the fluid unit 1 are shown in Fig. 14.

It can be seen from Fig. 14 that with the continuous increase of the fluid pulsation frequency, the amplitude of the main resonance of the fluid unit 1 fluctuates within a small range, which can be regarded as no changes; the amplitude
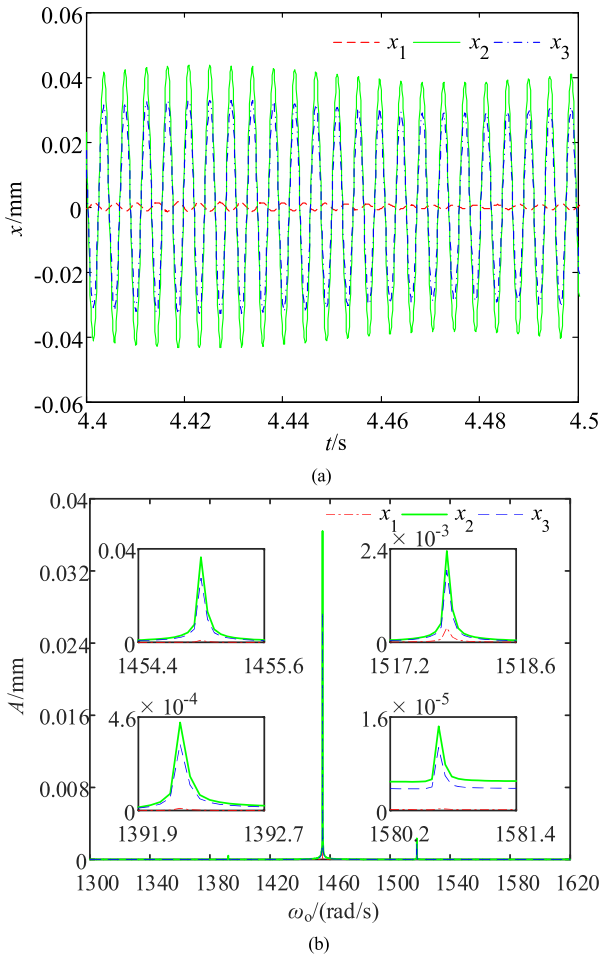
FIGURE 8. Combined resonance response jet system when ω_f is 10Hz. (a) time domain response. (b) frequency domain response.
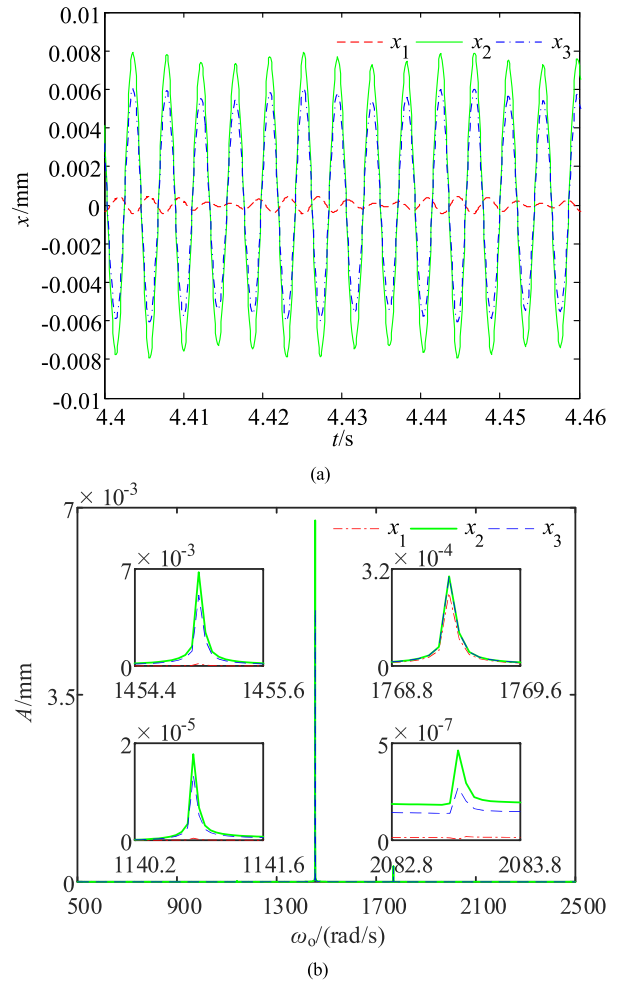

FIGURE 9. Combined resonance response jet system when ω_f is 50Hz. (a) time domain response. (b) frequency domain response.

of the combined resonance decreases gradually and varies greatly. In Fig. 14, the maximum amplitude of the combined resonance is 0.4335 mm, and the minimum value is 0.051 mm. The curves show that the change of fluid pulsation frequency rarely affects the main resonance of the jet system, but it has a greater impact on the combined resonance.

B. INFLUENCE OF AIR INLET RATE ON PARAMETER VIBRATION RESPONSE OF JET SYSTEM

When the air inlet rate continuously changes with other parameters unchanged and the external excitation frequency is close to the first natural frequency and the combined frequency between the first natural frequency and the fluid pulsation frequency respectively, the variation curves of the main resonance and combined resonance amplitude of the fluid unit 1 are shown in Fig. 15.

It can be seen from Fig. 15 that with the continuous increase of the air inlet rate, the amplitude of the main resonance of the jet system gradually increases and the amplitude of the combined resonance decreases gradually. In Fig. 15, the maximum amplitude of the main resonance is 0.6093 mm, and the minimum value is 0.3054 mm, and the maximum

amplitude of the combined resonance is 0.127 mm, and the minimum value is 0.0806 mm. The curves show that the change of air inlet rate has larger effects on the amplitude of parameter vibration of the jet system.

C. INFLUENCE OF FLUID PRESSURE ON PARAMETER VIBRATION RESPONSE OF JET SYSTEM

When the fluid pressure continuously changes with other parameters unchanged and the external excitation frequency is close to the first natural frequency and the combined frequency between the first natural frequency and the fluid pulsation frequency respectively, the variation curves of the main resonance and combined resonance amplitude of the fluid unit 1 are shown in Fig. 16.

It can be seen from Fig. 16 that with the continuous increase of the fluid pressure, both the amplitudes of the main resonance and the combined resonance of the jet system decrease gradually. In Fig. 16, the maximum amplitude of the main resonance is 0.4117 mm, and the minimum value is 0.2567 mm, and the maximum amplitude of the combined resonance is 0.1617 mm, and the minimum value is
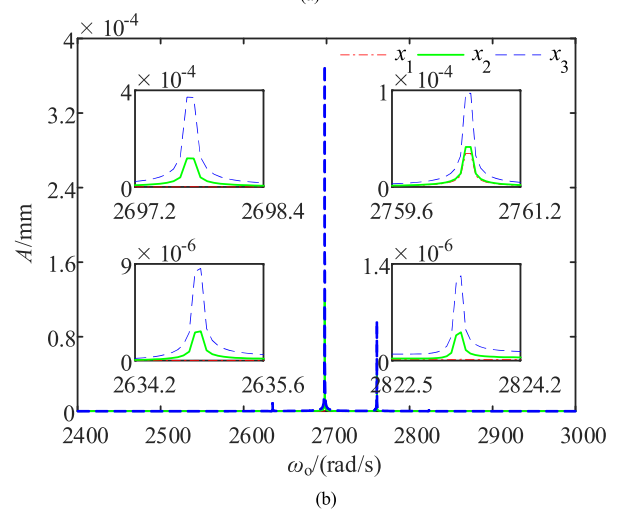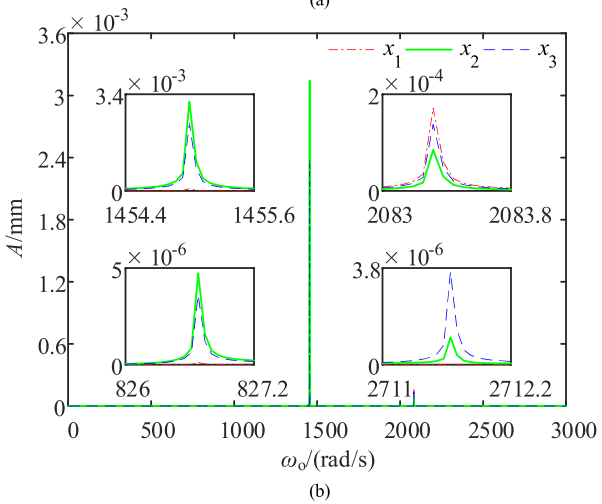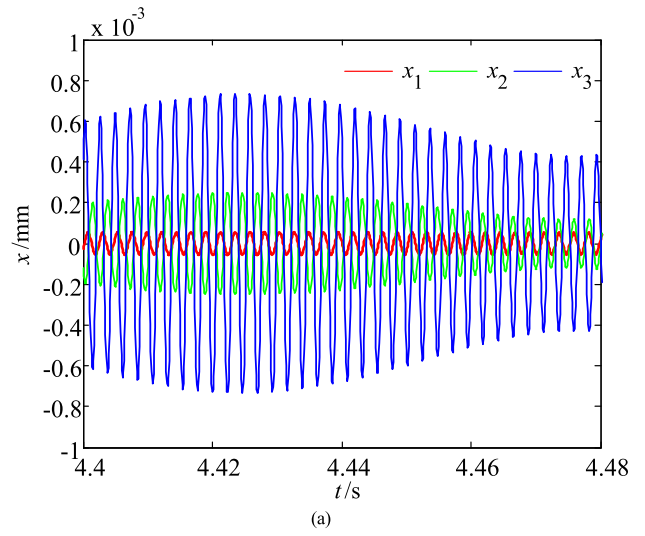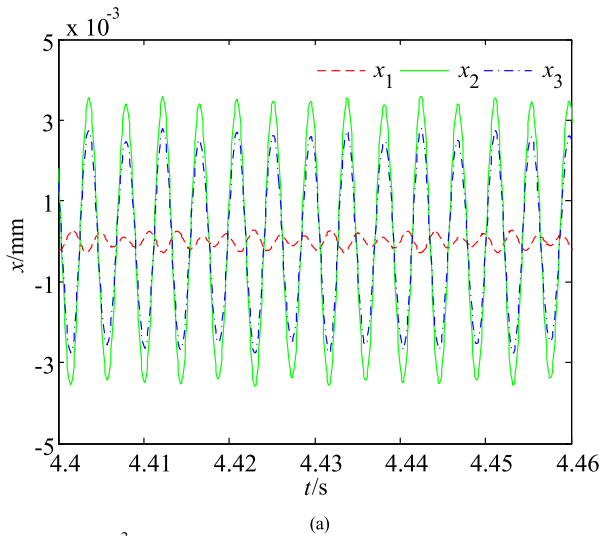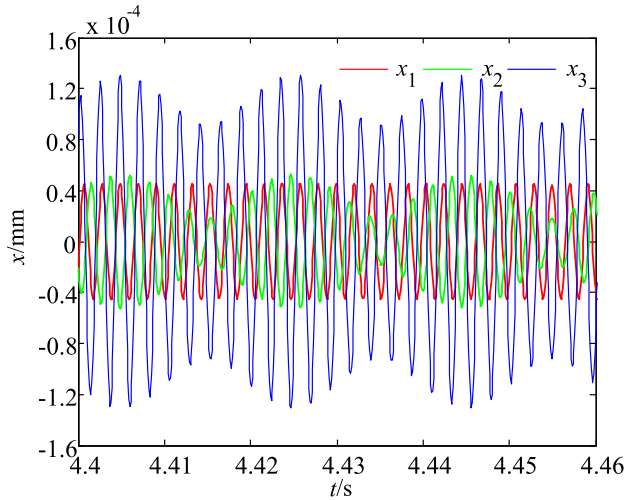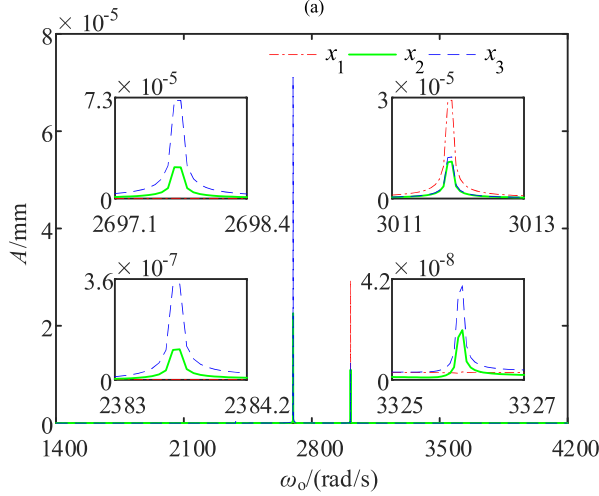
FIGURE 10. Combined resonance response jet system when ω_f is 100Hz. (a) time domain response. (b) frequency domain response.

FIGURE 11. Combined resonance response jet system when ω_f is 10Hz. (a) time domain response. (b) frequency domain response.

0.0669 mm. The curves show that the change of fluid pressure has larger effects on the amplitude of parameter vibration of the jet system.

D. INFLUENCE OF SPRAY CORE QUALITY ON PARAMETER VIBRATION RESPONSE OF JET SYSTEM

When the spray core quality continuously changes with other parameters unchanged and the external excitation frequency is close to the first natural frequency and the combined frequency between the first natural frequency and the fluid pulsation frequency respectively, the variation curves of the main resonance and combined resonance amplitude of the fluid unit 1 are shown in Fig. 17.

It can be seen from Fig. 17 that with the continuous increase of the spray core quality, both the amplitudes of the main resonance and the combined resonance of the jet system decrease gradually. In Fig. 17, the maximum amplitude of the main resonance is 0.3468 mm, and the minimum value is 0.3452 mm, and the maximum amplitude of the combined resonance is 0.1214 mm, and the minimum value
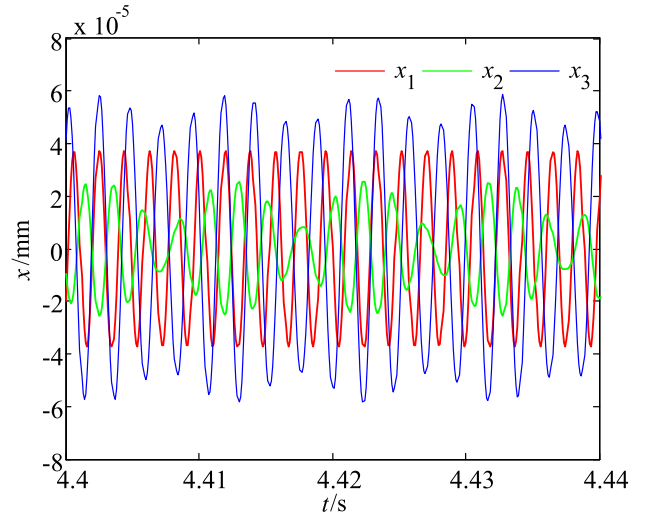
is 0.1196 mm. The curves show that the change of spray core quality has lower effects on the amplitude of parameter vibration of the jet system.

E. INFLUENCE OF MECHANICAL SPRING STIFFNESS ON PARAMETER VIBRATION RESPONSE OF JET SYSTEM

When the mechanical spring stiffness continuously changes with other parameters unchanged and the external excitation frequency is close to the first natural frequency and the combined frequency between the first natural frequency and the fluid pulsation frequency respectively, the variation curves of the main resonance and combined resonance amplitude of the fluid unit 1 are shown in Fig. 18.

It can be seen from Fig. 18 that with the continuous increase of the mechanical spring stiffness, both the amplitudes of the main resonance and the combined resonance of the jet system decrease gradually. In Fig. 18, the maximum amplitude of the main resonance is 0.3534 mm, and the minimum value is 0.3354 mm, and the maximum amplitude of the combined resonance is 0.1234 mm, and the minimum

FIGURE 12. Combined resonance response jet system when ω_f is 50Hz. (a) time domain response. (b) frequency domain response.

FIGURE 13. Combined resonance response jet system when ω_f is 100Hz. (a) time domain response. (b) frequency domain response.

value is 0.1163 mm. The curves show that the change of mechanical spring stiffness has lower effects on the amplitude of parameter vibration of the jet system.
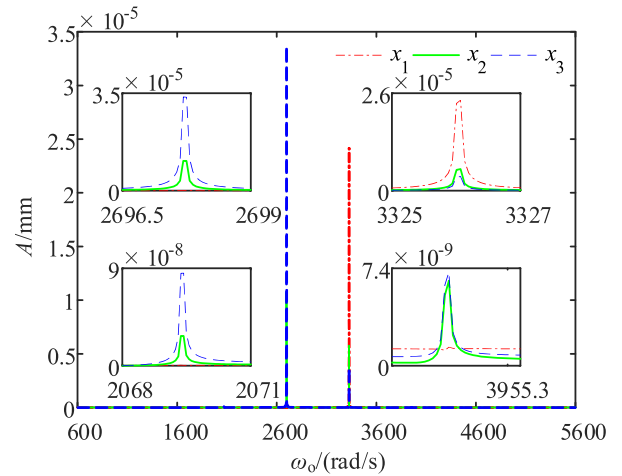
F. INFLUENCE OF FLUID DAMPING ON PARAMETER VIBRATION RESPONSE OF JET SYSTEM

When the fluid damping continuously changes with other parameters unchanged and the external excitation frequency is close to the first natural frequency and the combined frequency between the first natural frequency and the fluid pulsation frequency respectively, the variation curves of the main resonance and combined resonance amplitude of the fluid unit 1 are shown in Fig. 19.

It can be seen from Fig. 19 that as the fluid damping increases, the amplitude of the main resonance of the jet system remains basically unchanged, and the amplitude of the combined resonance gradually decreases. In Fig. 19, the amplitude of the main resonance remains basically unchanged at 0.3459 mm, and the maximum amplitude of the combined resonance is 0.1203 mm, and the minimum
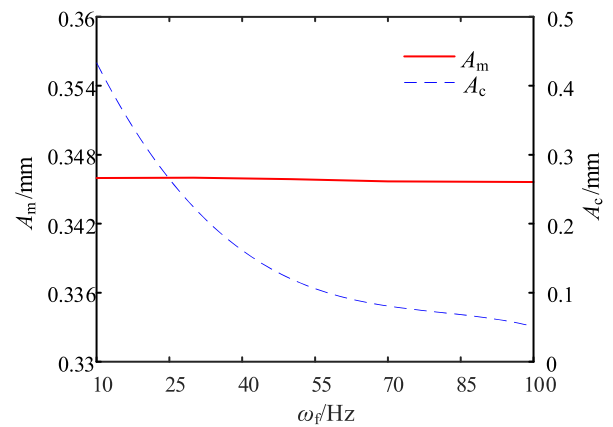

FIGURE 14. Amplitude variation of parameter vibration of the jet system under different fluid pulsation frequencies.

value is 0.1115 mm. The curves show that the change of fluid damping has basically no effect on the amplitude of the main
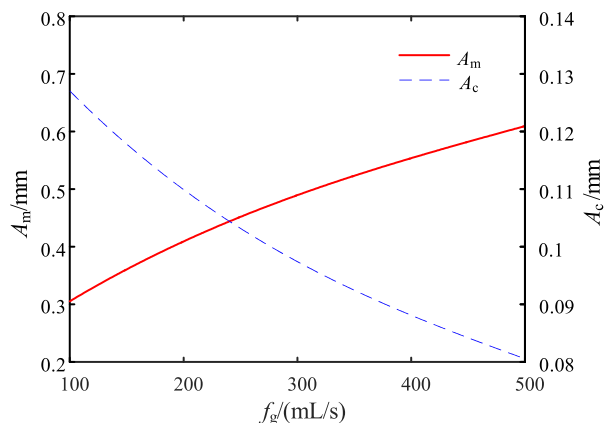
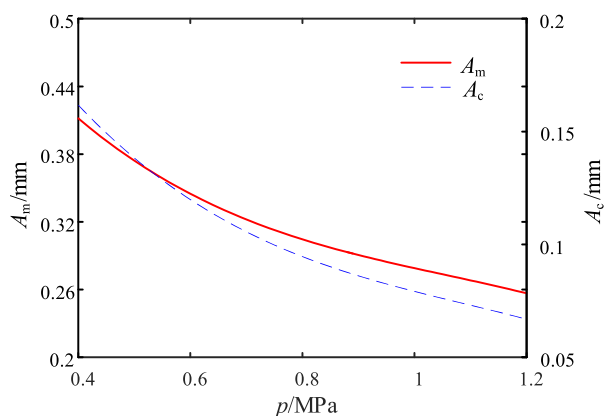**FIGURE 15.** Amplitude variation of parameter vibration of the jet system under different air inlet rates.

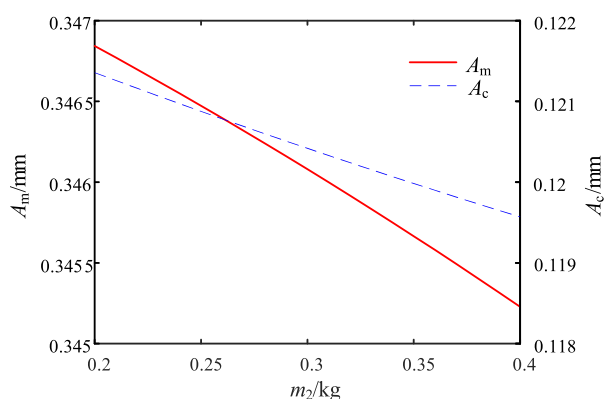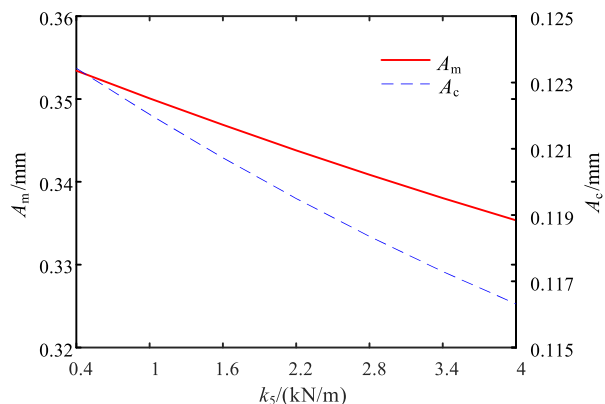**FIGURE 16.** Amplitude variation of parameter vibration of the jet system under different fluid pressure.

FIGURE 17. Amplitude variation of parameter vibration of the jet system under different spray core qualities.

FIGURE 18. Amplitude variation of parameter vibration of the jet system under different mechanical spring stiffness.
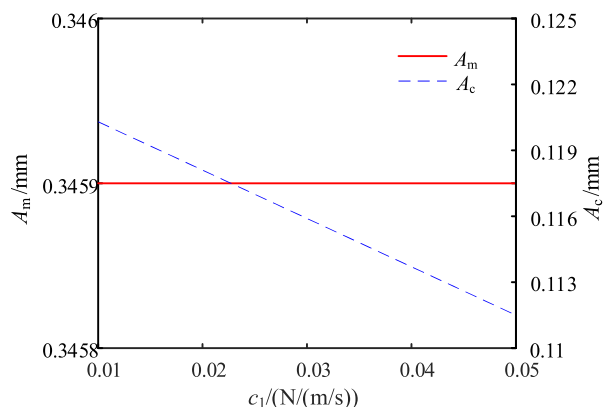

FIGURE 19. Amplitude variation of parameter vibration of the jet system under different fluid damping.

frequency between the first natural frequency and the fluid pulsation frequency respectively, the variation curves of the main resonance and combined resonance amplitude of the fluid unit 1 are shown in Fig. 20.
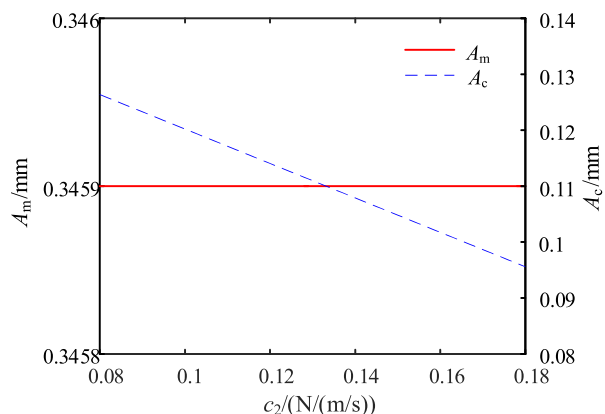

FIGURE 20. Amplitude variation of parameter vibration of the jet system under different structure damping.

resonance, but has a greater impact on the amplitude of the combined resonance.

G. INFLUENCE OF STRUCTURE DAMPING ON PARAMETER VIBRATION RESPONSE OF JET SYSTEM

When the structure damping continuously changes with other parameters unchanged and the external excitation frequency is close to the first natural frequency and the combined

It can be seen from Fig. 20 that as the structure damping increases, the amplitude of the main resonance of the jet system remains basically unchanged, and the amplitude of the combined resonance gradually decreases. In Fig. 20,

the amplitude of the main resonance remains basically unchanged at 0.3459 mm, and the maximum amplitude of the combined resonance is 0.1264 mm, and the minimum value is 0.09558 mm. The curves show that the change of structure damping has basically no effect on the amplitude of the main resonance, but has a greater impact on the amplitude of the combined resonance.

H. INFLUENCE OF PIPELINE LENGTH ON PARAMETER VIBRATION RESPONSE OF JET SYSTEM

When the pipeline length continuously changes with other parameters unchanged and the external excitation frequency is close to the first natural frequency and the combined frequency between the first natural frequency and the fluid pulsation frequency respectively, the variation curves of the main resonance and combined resonance amplitude of the fluid unit 1 are shown in Fig. 21.
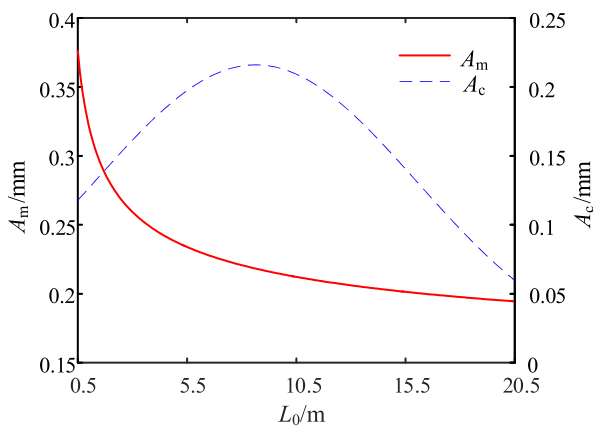

FIGURE 21. Amplitude variation of parameter vibration of the jet system under different pipeline length.

It can be seen from Fig. 21 that with the increase of the pipeline length, the amplitude of the main resonance decreases gradually, and the amplitude of the combined resonance of the jet system increases first and then decreases. In Fig. 21, the maximum amplitude of the main resonance is 0.3762 mm, and the minimum value is 0.1945 mm, and the maximum amplitude of the combined resonance is 0.216 mm, and the minimum value is 0.0596 mm. The curves show that the change of pipeline length has larger effects on the amplitude of parameter vibration of the jet system.

Based on the above analysis results, it can be seen that in the parameter vibration of the jet system, fluid parameters including fluid pulsation frequency, air inlet rate, fluid pressure, and fluid damping, mechanical parameters including spray core quality, mechanical spring stiffness, structural damping, and pipeline length, and the difference value between the external excitation frequency and the natural frequency and the combined frequency have effects on the main resonance and combined resonance of the jet system, and the influence law is complicated. Mass and stiffness are the main factors that affect the natural frequency of the jet system. The change in a certain parameter of the jet system may only cause

the change of mass or stiffness, or it may cause a simultaneous change of the two factors. Therefore, the influence of the change of the parameters of the jet system on its amplitude should consider the factors of mass and stiffness. Within the variation range of design parameters, we can sort these design parameters by the extent of the main resonance amplitude impact, and the order is: the air inlet rate, the pipeline length, the fluid pressure, the mechanical spring stiffness, the spray core quality, the fluid pulsation frequency, the fluid damping, and the structural damping, in which the air inlet rate has the largest influence, and the fluid damping and the structural damping have the least influence. Similarly, the order sorted by the extent of the combined resonance amplitude impact is: the fluid pulsation frequency, the pipeline length, the fluid pressure, the air inlet rate, the structural damping, the fluid damping, the mechanical spring stiffness, and the spray core quality, in which the fluid pulsation frequency has the greatest effect, and the spray core quality has the smallest impact.

V. CONCLUSIONS

1. The multi-scale method was used to solve the parameter vibration equation of the adaptive gun head jet system of the fire-fighting monitor. From the influence law of the fluid pulsation frequency on the amplitude of the jet system, it can be seen that when combination resonance exists, the range of the resonance frequency will be significantly expanded, especially when the fluid pulsation frequency or other excitation frequency components vary greatly, which makes dynamic behaviors of the jet system become more complicated.

2. Expect for the fluid pulsation frequency, the influence laws of the air inlet rate, the fluid pressure, the spray core quality, the mechanical spring stiffness, the fluid damping, the structural damping, and teh pipeline length on the amplitude of the jet system were also analyzed. From the extent of the amplitude impact, the air inlet rate has the greatest influence on the main resonance, and the fluid pulsation frequency has the greatest impact on the combined resonance.

3. In the parameter vibration of the jet system, fluid parameters including fluid pulsation frequency, air inlet rate, fluid pressure, and fluid damping, mechanical parameters including spray core quality, mechanical spring stiffness, structural damping, and pipeline length, and the difference value between the external excitation frequency and the natural frequency and the combined frequency have effects on the main resonance and combined resonance of the jet system, and the influence law is complicated.

REFERENCES

[1] X. Yuan, X. Zhu, C. Wang, L. Zhang, and Y. Zhu, "Natural frequency sensitivity analysis of fire-fighting jet system with adaptive gun head," *Processes*, vol. 7, no. 11, p. 808, Nov. 2019, doi: 10.3390/pr7110808.

[2] R. H. Gallucci, "Risk-reduction credit for very early warning fire detection at nuclear power plants: From FAQ to fiction," *Civil Eng. J.*, vol. 5, no. 2, p. 309, Feb. 2019, doi: 10.28991/cej-2019-03091246.

[3] W. T. Dai, J. X. Jiang, G. F. Ding, and Z. G. Liu, "Development and application of fire video image detection technology in China's road tunnels," *Civil Eng. J.*, vol. 5, no. 1, pp. 1–17, Jan. 2019, doi: 10.28991/cej-2019-03091221.

[4] X. Yuan, X. Zhu, C. Wang, and L. Zhang, "Research on theoretical model of dynamic bulk modulus of gas-containing hydraulic oil," *IEEE Access*, vol. 7, pp. 178413–178422, Dec. 2019, doi: 10.1109/ACCESS.2019.2959058.

[5] Y. Zhang, J. Zhao, B. Grabrick, B. Jacobson, A. Nelson, and J. Otte, "Dynamic response of three floaters supporting vertical axis wind turbines due to wind excitation," *J. Fluids Struct.*, vol. 80, pp. 316–331, Jul. 2018, doi: 10.1016/j.jfluidstructs.2018.04.003.

[6] J. Zhang, Q.-G. Wang, and J. Sun, "On finite-time stability of nonautonomous nonlinear systems," *Int. J. Control*, vol. 93, no. 4, pp. 783–787, Apr. 2020, doi: 10.1080/00207179.2018.1536831.

[7] J. A. Souza and L. H. Takamoto, "Lyapunov stability for impulsive control affine systems," *J. Differ. Equ.*, vol. 266, no. 7, pp. 4232–4267, Mar. 2019, doi: 10.1016/j.jde.2018.09.033.

[8] V. Pravec, "Remarks on definitions of periodic points for nonautonomous dynamical system," *J. Difference Equ. Appl.*, vol. 25, nos. 9–10, pp. 1372–1381, Oct. 2019, doi: 10.1080/10236198.2019.1641496.

[9] X. Yuan, X. Zhu, C. Wang, and L. Zhang, "Nonlinear dynamics of adaptive gun head jet system of fire-fighting monitor," *IEEE Access*, vol. 8, pp. 75210–75222, Apr. 2020, doi: 10.1109/ACCESS.2020.2988912.

[10] S. Tang, S. Yuan, and Y. Zhu, "Deep learning-based intelligent fault diagnosis methods toward rotating machinery," *IEEE Access*, vol. 8, pp. 9335–9346, Dec. 2020, doi: 10.1109/ACCESS.2019.2963092.

[11] Y. Zhu, S. N. Tang, L. X. Quan, W. L. Jiang, and L. Zhou, "Extraction method for signal effective component based on extreme-point symmetric mode decomposition and Kullback–Leibler divergence," *J. Brazilian Soc. Mech. Sci. Eng.*, vol. 41, no. 2, p. 100, Feb. 2019, doi: 10.1007/s40430-019-1599-9.

[12] W. Li, E. Li, L. Ji, L. Zhou, W. Shi, and Y. Zhu, "Mechanism and propagation characteristics of rotating stall in a mixed-flow pump," *Renew. Energy*, vol. 153, pp. 74–92, Jun. 2020, doi: 10.1016/j.renene.2020.02.003.

[13] D. Li, H. Wang, Z. Li, T. K. Nielsen, R. Goyal, X. Wei, and D. Qin, "Transient characteristics during the closure of guide vanes in a pump-turbine in pump mode," *Renew. Energy*, vol. 118, pp. 973–983, Apr. 2018, doi: 10.1016/j.renene.2017.10.088.

[14] S. Zhang, M. Clark, X. Liu, D. Chen, P. Thomas, and L. Ren, "The effects of bio-inspired electromagnetic fields on healthy enhancement with case studies," *Emerg. Sci. J.*, vol. 3, no. 6, pp. 369–381, Dec. 2019, doi: 10.28991/esj-2019-01199.

[15] L. Lyu, Z. Chen, and B. Yao, "Energy saving motion control of independent metering valves and pump combined hydraulic system," *IEEE/ASME Trans. Mechatronics*, vol. 24, no. 5, pp. 1909–1920, Oct. 2019, doi: 10.1109/TMECH.2019.2930276.

[16] X. Yuan, X. Zhu, C. Wang, L. Zhang, and Y. Zhu, "Research on the dynamic behaviors of the jet system of adaptive fire-fighting monitors," *Processes*, vol. 7, no. 12, p. 952, Dec. 2019, doi: 10.3390/pr7120952.

[17] Y. Zhu, S. Tang, C. Wang, W. Jiang, X. Yuan, and Y. Lei, "Bifurcation characteristic research on the load vertical vibration of a hydraulic automatic gauge control system," *Processes*, vol. 7, no. 10, p. 718, Oct. 2019, doi: 10.3390/pr7100718.

[18] Y. Zhu, P. Qian, S. Tang, W. Jiang, W. Li, and J. Zhao, "Amplitude-frequency characteristics analysis for vertical vibration of hydraulic AGC system under nonlinear action," *AIP Adv.*, vol. 9, no. 3, Mar. 2019, Art. no. 035019, doi: 10.1063/1.5085854.

[19] Y. Zhu, S. N. Tang, C. Wang, W. L. Jiang, J. H. Zhao, and G. P. Li, "Absolute stability condition derivation for position closed-loop system in hydraulic automatic gauge control," *Processes*, vol. 7, no. 10, p. 766, Oct. 2019, doi: 0.3390/pr7100766.

[20] L. Lyu, Z. Chen, and B. Yao, "Advanced valves and pump coordinated hydraulic control design to simultaneously achieve high accuracy and high efficiency," *IEEE Trans. Control Syst. Technol.*, early access, Feb. 25, 2020, doi: 10.1109/tcst.2020.2974180.

[21] L. Lyu, Z. Chen, and B. Yao, "Development of pump and valves combined hydraulic system for both high tracking precision and high energy efficiency," *IEEE Trans. Ind. Electron.*, vol. 66, no. 9, pp. 7189–7198, Sep. 2019, doi: 10.1109/TIE.2018.2875666.

[22] J. Yao and W. Deng, "Active disturbance rejection adaptive control of hydraulic servo systems," *IEEE Trans. Ind. Electron.*, vol. 64, no. 10, pp. 8023–8032, Oct. 2017, doi: 10.1109/TIE.2017.2694382.

[23] Z. Yao, J. Yao, and W. Sun, "Adaptive RISE control of hydraulic systems with multilayer neural-networks," *IEEE Trans. Ind. Electron.*, vol. 66, no. 11, pp. 8638–8647, Nov. 2019, doi: 10.1109/TIE.2018.2886773.

[24] S. Yoo, C.-G. Park, and S.-H. You, "Inertial parameter estimation for the dynamic simulation of a hydraulic excavator," *J. Mech. Sci. Technol.*, vol. 32, no. 9, pp. 4045–4056, Sep. 2018, doi: 10.1007/s12206-018-0804-6.

[25] S. Quayyum, "Refined parametric models for wind load resistances of wood-frame walls," *Eng. Struct.*, vol. 183, pp. 841–859, Mar. 2019, doi: 10.1016/j.engstruct.2019.01.058.

[26] J. Kato, T. Inoue, K. Takagi, and S. Yabui, "Nonlinear analysis for influence of parametric uncertainty on the stability of rotor system with active magnetic bearing using feedback linearization," *J. Comput. Nonlinear Dyn.*, vol. 13, no. 7, Jul. 2018, Art. no. 071004, doi: 10.1115/1.4040128.

[27] J. Pei, W. J. Wang, and S. Q. Yuan, "Multi-point optimization on meridional shape of a centrifugal pump impeller for performance improvement," *J. Mech. Sci. Technol.*, vol. 30, no. 11, pp. 4930–4949, Nov. 2016, doi: 10.1007/s12206-016-1015-7.

[28] E. Galvan, R. J. Malak, D. J. Hartl, and J. W. Baur, "Performance assessment of a multi-objective parametric optimization algorithm with application to a multi-physical engineering system," *Struct. Multidisciplinary Optim.*, vol. 58, no. 2, pp. 489–509, Aug. 2018, doi: 10.1007/s00158-018-1902-x.

[29] X. Liu and J. Luo, "A dynamic multi-objective optimization model with interactivity and uncertainty for real-time reservoir flood control operation," *Appl. Math. Model.*, vol. 74, pp. 606–620, Oct. 2019, doi: 10.1016/j.apm.2019.05.009.

[30] V. Rafiee and J. Faiz, "Robust design of an outer rotor permanent magnet motor through six-sigma methodology using response surface surrogate model," *IEEE Trans. Magn.*, vol. 55, no. 10, pp. 1–10, Oct. 2019, doi: 10.1109/TMAG.2019.2923160.

[31] E. Hazir and T. Ozcan, "Response surface methodology integrated with desirability function and genetic algorithm approach for the optimization of CNC machining parameters," *Arabian J. Sci. Eng.*, vol. 44, no. 3, pp. 2795–2809, Mar. 2019, doi: 10.1007/s13369-018-3559-6.

[32] T. Mukhopadhyay, S. Chakraborty, S. Dey, S. Adhikari, and R. Chowdhury, "A critical assessment of kriging model variants for high-fidelity uncertainty quantification in dynamics of composite shells," *Arch. Comput. Methods Eng.*, vol. 24, no. 3, pp. 495–518, Jul. 2017, doi: 10.1007/s11831-016-9178-z.

[33] P. Ni, J. Li, H. Hao, W. Yan, X. Du, and H. Zhou, "Reliability analysis and design optimization of nonlinear structures," *Rel. Eng. Syst. Saf.*, vol. 198, Jun. 2020, Art. no. 106860, doi: 10.1016/j.ress.2020.106860.

XIAOMING YUAN received the B.S. and Ph.D. degrees from the School of Mechanical Engineering, Yanshan University, Qinhuangdao, China, in 2008 and 2014, respectively. He was a Post-Doctoral with the XCMG Construction Machinery from 2015 to 2018. Since 2015, he has been a Lecture with the School of Mechanical Engineering, Yanshan University. He is currently a Senior Member of the Chinese Mechanical Engineering Society (CEMS). His research interests include fluid-structure interaction dynamics of fire-fighting monitor, fluid transmission and control, and new magnetic gear transmission and control.

XUAN ZHU received the B.S. degree from the School of Mechanical Engineering, Yanshan University, Qinhuangdao, China, in 2018, where he is currently pursuing the master's degree. His research interests include fluid transmission and control and fluid system simulation.
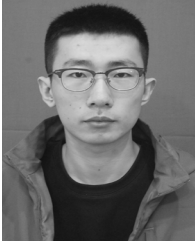
CHU WANG received the B.S. degree from the College of Mechatronic Engineering, North University of China, Taiyuan, China, in 2017. He is currently pursuing the master's degree with the School of Mechanical Engineering, Yanshan University, Qinhuangdao, China. His research interests include fluid transmission and control and fluid system simulation.

LIJIE ZHANG received the B.S., M.S., and the Ph.D. degrees from the School of Mechanical Engineering, Yanshan University, Qinhuangdao, China. He has been a Professor with the School of Mechanical Engineering, Yanshan University, since 2008, and became the Ph.D. Tutor in 2008. He was a Senior Visiting Scholar with the Iowa State University of Science and Technology in 2009. He is currently a Senior Member of the Chinese Mechanical Engineering Society (CEMS) and a Review Expert of the National Natural Science Foundation of China (NSFC). His research interests include reliability and fault diagnosis of hydraulic components, multiphysics coupling analysis, and mechanics and robotics.

• • •